



Loss of selenoprotein W in murine macrophages alters the hierarchy of selenoprotein expression, redox tone, and mitochondrial functions during inflammation

Sougat Misra^a, Tai-Jung Lee^a, Aswathy Sebastian^b, John McGuigan^a, Chang Liao^c, Imhoi Koo^d, Andrew D. Patterson^{a,d}, Randall M. Rossi^e, Molly A. Hall^a, Istvan Albert^b, K. Sandeep Prabhu^{a,*}

^a Department of Veterinary and Biomedical Sciences, Center for Molecular Immunology and Infectious Disease, The Pennsylvania State University, University Park, PA, 16802, USA

^b Bioinformatics Core, Huck Institute of the Life Sciences, The Pennsylvania State University, University Park, PA, 16802, USA

^c Department of Medicine- Infectious Diseases, University of California, San Francisco, CA, 94143, USA

^d Metabolomics Core Facility, Huck Institute of the Life Sciences, The Pennsylvania State University, University Park, PA, 16802, USA

^e Transgenic Mouse Core Facility, Huck Institute of the Life Sciences, The Pennsylvania State University, University Park, PA, 16802, USA

ARTICLE INFO

Keywords:

Reactive oxygen species
Mitochondrial respiration
Metabolism
Glycolysis
Krebs cycle
Energy metabolism
Arginase
Sik2
Resolution

ABSTRACT

Macrophages play a pivotal role in mediating inflammation and subsequent resolution of inflammation. The availability of selenium as a micronutrient and the subsequent biosynthesis of selenoproteins, containing the 21st amino acid selenocysteine (Sec), are important for the physiological functions of macrophages. Selenoproteins regulate the redox tone in macrophages during inflammation, the early onset of which involves oxidative burst of reactive oxygen and nitrogen species. SELENOW is a highly expressed selenoprotein in bone marrow-derived macrophages (BMDMs). Beyond its described general role as a thiol and peroxide reductase and as an interacting partner for 14-3-3 proteins, its cellular functions, particularly in macrophages, remain largely unknown. In this study, we utilized *Selenow* knock-out (KO) murine bone marrow-derived macrophages (BMDMs) to address the role of SELENOW in inflammation following stimulation with bacterial endotoxin lipopolysaccharide (LPS). RNAseq-based temporal analyses of expression of selenoproteins and the Sec incorporation machinery genes suggested no major differences in the selenium utilization pathway in the *Selenow* KO BMDMs compared to their wild-type counterparts. However, selective enrichment of oxidative stress-related selenoproteins and increased ROS in *Selenow*^{-/-} BMDMs indicated anomalies in redox homeostasis associated with hierarchical expression of selenoproteins. *Selenow*^{-/-} BMDMs also exhibited reduced expression of arginase-1, a key enzyme associated with anti-inflammatory (M2) phenotype necessary to resolve inflammation, along with a significant decrease in efferocytosis of neutrophils that triggers pathways of resolution. Parallel targeted metabolomics analysis also confirmed an impairment in arginine metabolism in *Selenow*^{-/-} BMDMs. Furthermore, *Selenow*^{-/-} BMDMs lacked the ability to enhance characteristic glycolytic metabolism during inflammation. Instead, these macrophages atypically relied on oxidative phosphorylation for energy production when glucose was used as an energy source. These findings suggest that SELENOW expression in macrophages may have important implications on cellular redox processes and bioenergetics during inflammation and its resolution.

1. Introduction

Oxidative redox metabolism is a hallmark of inflammatory responses. Reactive oxygen (ROS) and nitrogen species (RNS) play important roles in diverse cellular processes including antimicrobial

activity, redox regulation of immune signaling, and the inflammasome activation among others key pathways important for the optimal functioning of the innate immune system [1]. While these reactive metabolic intermediates are important to mount inflammatory response, their elimination is also essential to avoid cellular damage afforded due to

* Corresponding author.

E-mail address: ksp4@psu.edu (K.S. Prabhu).

<https://doi.org/10.1016/j.redox.2022.102571>

Received 20 November 2022; Accepted 4 December 2022

Available online 8 December 2022

2213-2317/© 2022 The Authors. Published by Elsevier B.V. This is an open access article under the CC BY-NC-ND license (<http://creativecommons.org/licenses/by-nc-nd/4.0/>).

their inherent and indiscriminate reactivity towards macromolecules [2]. Exacerbation of inflammation requires mounting an altered state of redox buffering capacity in innate immune cells, specifically macrophages, to counteract inflammation-associated redox stress. In this context, selenoproteins play an important role mainly as disulfide and peroxide reductases, and methionine sulfoxide reductase [3]. We and others have demonstrated that the availability of selenium and selenoprotein expression are important for both the propagation of inflammatory signals and initiation of timely resolution of inflammation [4–9]. In addition, redox processes are intricately involved in the metabolic reprogramming required to meet the increased cellular energy demand during inflammation and active resolution [10]. It is likely that any perturbations of the redox-regulatory signaling pathways may have significant impact on the inflammatory response and subsequent resolution of inflammation, potentially delaying the transition to homeostasis. While the involvement of several mammalian selenoproteins are well-established in the context of inflammation [reviewed in 5, 11], there is limited understanding on the role of SELENOW in macrophages. The inherent plasticity of macrophages is associated with metabolic adaptations that sustain their polarization towards a pro-inflammatory (M1) or anti-inflammatory (M2) phenotype, which is regulated by diverse factors, including cytokines, bioactive lipid mediators, as well as efferocytosis of apoptotic neutrophils. To this end, previous studies demonstrated that *Selenow* mRNA [12] and protein [13] were highly expressed in bone marrow-derived macrophages (BMDMs) in response to exogenous selenium supply.

SELENOW is a small (9.32 kD) selenoprotein with a classical selenocysteine (Sec)-containing thioredoxin motif (C-X-X-U) in the N-terminus that is implicated in its reductase activity [14]. In addition, the Sec residue has been implicated in its non-canonical interaction with 14-3-3 protein [15]. Seven isoforms of 14-3-3 family of proteins function as rheostats of diverse cellular processes, mainly as interacting partners with different classes proteins [16]. Through diverse mechanisms, 14-3-3 family of proteins regulate NF- κ B, JAK-STAT, PPAR, and glucocorticoid receptor signaling pathways, which play distinct roles in inflammation and resolution [reviewed in 17]. In addition, SELENOW positively regulates mTORC2 activity (in complex with Rictor) upon binding with 14-3-3 [18], resulting in the phosphorylation of AKT, a key mediator of the insulin/PI3K signaling axis. Therefore, the loss of SELENOW may directly impact the mTORC2-mediated activation of AKT [19] and subsequent metabolic reprogramming associated with inflammatory response.

In this study, we interrogated whether the genetic ablation of *Selenow* impacts selenium utilization pathway, inflammatory response, redox tone, and cellular energetics by utilizing BMDMs under selenium-replete conditions. In addition, we investigated the dynamic changes in selenoprotein gene and protein expression profiles involving sterile inflammation to evaluate the selenium utilization pathway either in the presence or absence of SELENOW. Our findings suggest that the loss of SELENOW in BMDMs impacted the expression of several key selenoproteins during LPS-induced acute inflammation. *Selenow*^{-/-} macrophages expressed lower levels of ARG1 and its downstream metabolite, ornithine, essential for resolution of inflammation that was corroborated by decreased efferocytosis of neutrophils. Interestingly, *Selenow*^{-/-} macrophages exhibited augmented mitochondrial respiration and lacked the characteristic increase in glycolysis during early inflammation, suggesting the disruption of canonical metabolic switching associated with the loss of SELENOW. Our study highlights a previously unrecognized role of SELENOW in regulating glucose and arginine metabolism in macrophages during inflammation.

2. Materials and Methods

Mice: Eight to twelve weeks old C57BL/6 mice (Taconic Biosciences, USA) were used for all the experiments. *Selenow* knockout mice were generated in-house at the Transgenic Core, Penn State University, using

CRISPR/Cas9 system. Murine SelenoW sgRNA sequence was designed using the MIT CRISPR-Cas9 design tool (<http://crispr.mit.edu>). A sequence with score >85 with minimum off-targets was selected. Mouse sgRNA lentivectors with puromycin and mCherry dual selection markers were purchased from VectorBuilder. The target sequence used was 5'-CTTCAAAGAACCCGGTGACC-3'. We used the lentiviral particles with this sgRNA in murine cells to validate the efficacy. A whole body SelenoW mutant mouse line (on a C57BL/6 background) was generated by microinjection of this pre-validated sgRNA in complex with recombinant Cas9 (New England Biolabs) into single cell embryos. Upon implantation and crossing the pups (F2 generation), PCR, surveyor assay, and sequencing was performed to confirm the mutation. Protein expression in the PBMCs and ear tissue was performed to confirm the lack of expression of SelenoW. Homozygous KO mice were backcrossed for 10 generations to confirm the germline deletion of the target gene. These homozygous SelenoW KO mice were genotyped to confirm the mutation on a regular basis. Study protocol involving all the animal procedures were approved by IACUC at The Pennsylvania State University.

CRISPR-Cas9-based whole body knock out strategy yielded complete loss of SELENOW at protein level (Fig. 1, bottom panel). *Selenow*^{-/-} mice were fertile with normal litter size. Loss of Selenow did not result in any overt phenotype under normal maintenance conditions.

2.1. Reagents

Isolation and culture of murine BMDMs: Femur and tibia were surgically resected from the hind legs of mice following CO₂ euthanasia. After removal of muscles and connective tissues, bones were flushed with ice-cold DMEM media using syringes fitted with 25-gauge needles. Cells were further mechanically dissociated following sequential flushing with 16- and 18-gauge needles. Single step centrifugation (300 g, 3 min at 4 °C) yielded cell pellets that were resuspended in complete BMDM culture media comprising of DMEM media supplemented with 10% (v/v) conditioned media from L929 culture, 100 nM sodium selenite, 5% defined FBS, 1X Penicillin-Streptomycin, and 1X L-glutamine. Cells were seeded in 35 mm dishes (BD Falcon), unless stated otherwise. Culture media was completely removed at every 48 h and replenished with fresh media. On day 5, greater than 95% adherent cells were F4/80⁺CD11b⁺ and were used as BMDMs for experiments. BMDMs were treated with *E. coli* LPS (Serotype: 0111: B4; 100 ng/ml; Sigma) for 1 h to induce sterile inflammation following which media was changed and replenished with fresh media. Cells or media samples were collected at indicated time points for subsequent analyses (Fig. 1).

RNA-sequencing: WT and *Selenow*^{-/-} macrophages were treated with LPS for 0, 4, 8, and 24 h (n = 3 for each time point). At the end of the treatment, culture media was removed, and cells were collected using cell scraper following a single wash with ice-cold PBS. Total RNA was isolated using RNeasy Plus Mini Kit (Qiagen) with on column DNase treatment to remove any traces of genomic DNA. Libraries were prepared from sample with RNA integrity (RIN) values exceeding 9.0 (Agilent 2100). One sample (*Selenow*^{-/-}, 24 h) was excluded from analyses due to low RIN value. Pair-ended (PE100) sequencing was carried out using DNBseq platform with minimum read depth of 40 M/sample (Beijing Genomics Institute, China). Mapping was done using hisat2 and abundance of mapped genes were quantified using featureCounts. Differential gene expression analysis was performed using DESeq2 pipeline in RStudio (V1.4.1717). Normalized expression of selected genes was extracted from the dataset for subsequent analyses.

RT-qPCR: Total RNA was isolated from cells using Trizol reagent (Sigma Aldrich, USA) and reverse transcribed with oligo-dT primer to synthesize cDNA. Ten nanogram of total cDNA was used as input for each RT-qPCR reactions and amplified using StepOnePlus Real-Time PCR instrument (Thermo Fisher). Validated TaqMan probes were used for target mRNA amplification. *Gapdh* served as internal control for relative quantitation of gene expression.

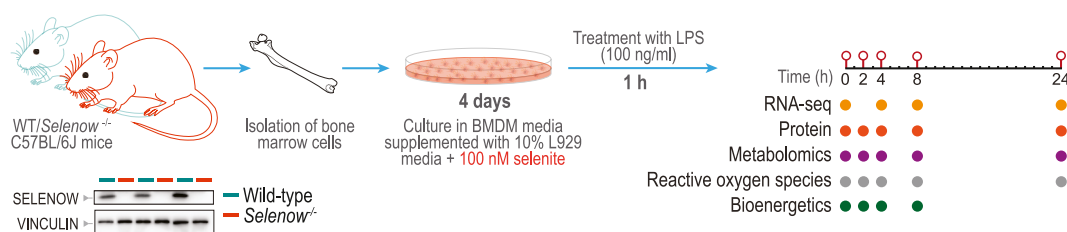


Fig. 1. A schematic illustration depicting the experimental design to elucidate the differences in inflammatory response in WT and *Selenow*^{-/-} BMDMs. The immunoblots confirms complete loss of SELENOW in *Selenow*^{-/-} BMDMs.

Western blot: Cell lysates were prepared using mammalian protein extraction reagent (MPER, Thermo Scientific) containing protease inhibitor cocktail and phosphatase inhibitor and centrifuged at 10,000 g for 20 min at 4 °C. Protein content in the cell lysates were determined using a BCA assay kit. Equal amount of protein under desaturating condition was run in SDS-PAGE gel (T = 12.5%), transferred into PVDF membrane, and probed with primary antibodies overnight at 8 °C. Appropriate HRP-conjugated secondary antibodies were used for chemiluminescent detection (West Pico chemiluminescence reagent, Thermo Scientific) of immuno-conjugated protein bands using G: BOX Chemi XX6 (Syngene) imaging system. Image J software (National Institutes of Health)-based analysis of band density was used for semi-quantitative protein expression. Expression of β -actin in the corresponding samples from the same blots were utilized for data normalization. Whenever possible, blots were stripped and reprobed to detect multiple target proteins from the same membrane.

Measurement of reactive oxygen species (ROS): We utilized CellRox Assay Kit (Thermo Scientific) for the detection of total ROS. Briefly, cells were harvested using a cell scraper after treatment with LPS at the indicated time points. Following a single wash, cells were stained with CellRox dye (final concentration, 5 μ M) in BMDM culture media at 37 °C for 30 min. This was followed by removal of the staining media and resuspension of the cells in cell staining buffer (Biolegend, USA) containing propidium iodide (PI, final concentration 0.7 μ g/ml) for 15 min. Stained cells were analyzed with BD Accuri flow cytometer (50,000 events/sample). Two different cell viability markers were used to resolve spectral overlap between the dyes. Data were analyzed using FlowJo software program (V10.8.0, BD Biosciences). Detailed gating strategy is included in Fig. S3.

Mitochondrial oxidative phosphorylation and glycolytic stress tests: A Seahorse XFe24 Bioanalyzer (Agilent) was used to determine oxygen consumption rate (OCR) and extracellular acidification rate (ECAR). Briefly, femur-originated whole bone marrow cells from WT and *Selenow*^{-/-} mice were seeded on to a 24-well Seahorse XFe24 cell culture microplate in 200 μ l BMDM culture media. After 96 h, cells were treated with LPS (100 ng/ml) at different time points for 1 h and culture media was removed and replenished with LPS-free fresh media. These experiments were designed such that cellular respiration in LPS-treated cells for different time points (0, 2, 4, and 8 h) can be measured in parallel. Experiments were run in pH-adjusted (7.40) Seahorse base assay medium containing 1.0 mM sodium pyruvate, 2.0 mM L-glutamine, and 10.0 mM D-glucose. Cellular respiration was measured at the baseline and in the presence oligomycin (1.0 μ M), FCCP (1.0 μ M), and rotenone + antimycin A (1.0 μ M each) - the concentrations which were empirically determined in range-finding experiments. The experimental set up for glycolytic stress test was similar except for that glucose-free base medium was used and D-glucose (10 mM), oligomycin (1.5 μ M), and 2-deoxyglucose (50 mM) were added sequentially to enumerate ECAR. At the end of each run, media from all the wells was aspirated carefully. Plates were sealed with parafilm and stored at -80 °C for subsequent quantification of total DNA using a CyQuant assay kit (Thermo Fisher, USA). Standard curve of total DNA was constructed from serial dilution of BMDMs and cell number in each well were back calculated from the measured DNA amount for data normalization.

Efferocytosis assay: BMDMs from WT and *Selenow*^{-/-} mice were cultured for 4 days, as described earlier with minor modifications [20]. Briefly, cells were mechanically harvested on day 5 and replated in 12-well plates (100,000 live cells/well). On the same day, polymorphonuclear neutrophils (PMNs) from WT mice femurs were isolated using the MojoSort™ Mouse Neutrophil Isolation Kit (Biolegend). After isolation, PMNs were counted and labeled with PKH26 red fluorescent cell linker mini kit for general cell membrane labeling (Sigma Aldrich) and cultured overnight in RPMI media containing 10% FBS, 2.5 mM HEPES, 1 mM CaCl₂ and 100 nM sodium selenite to induce spontaneous apoptosis. At the end of the culture period, PMNs were centrifuged at 700 g for 3 min, counted, resuspended in BMDM media. Five hundred PMNs were then added to each well of BMDMs. After 4 h, cells were washed twice with PBS to remove excess PMNs and BMDMs were harvested with cell scrapers. Cells were then resuspended in flow buffer (3% FBS in PBS). Fc receptors were blocked with purified rat anti-mouse CD16/CD32 (Mouse BD Fc Block™, BD Bioscience) for 10 min, followed by 30 min staining with APC-F4/80 (Miltenyi Biotec). After washing, samples were analyzed with Amnis FlowSight imaging flow cytometer. Efferocytosis were measured by the percentage of F4/80 and PKH26 double-positive macrophages out of total F4/80 positive macrophages.

Extraction and analyses of selective metabolites using LC/MS: Isolated bone marrow cells were cultured in 35 mm culture dish in glucose-free DMEM media supplemented with 4.5 g/L ¹³C₆-glucose (Sigma Aldrich) along with other supplements, as described earlier. Experiments were terminated at 0, 2, 4, 8, and 24 h post LPS treatment (100 ng/ml). Briefly, cells were washed twice with ice-cold PBS at the indicated time points and placed on dry ice for quenching metabolism. One ml of ice-cold 50% (v/v) acetonitrile was added to the cells and left at -80 °C for 10 min. Following thawing, cells were scrapped, collected, incubated at -20 °C for 20 min. The supernatants were centrifuged at 5000 g for 10 min at 4 °C and stored at -80 °C until further analyses. Metabolites in the samples were analyzed using Thermo Orbitrap Exactive Plus LC/MS in negative mode [21]. Identification of metabolites was performed using an in-house standards library with known precursor *m/z* and retention time and was annotated with precursor *m/z* in MoNA reference library. Data analysis was conducted using MS-DIAL [22]. Chlorpropamide was used as an internal standard and used for normalization of data.

Isolation of mitochondria: Liver samples were minced and homogenized in extraction buffer (0.25 M sucrose, 20 mM HEPES-KOH, pH 7.5, 10 mM KCl, 1.5 mM MgCl₂, 1.0 mM EDTA, 1.0 mM EGTA, 1.0 mM dithiothreitol, and 0.1 mM PMSF). Homogenized samples were centrifuged twice at 750 g for 10 min to collect the mitochondria in the supernatant followed by centrifugation at 10,000 g for 15 min to pellet down the mitochondria [23]. Isolated mitochondrial fractions were resuspended in the homogenization buffer (210 mM mannitol, 70 mM sucrose, 5 mM Tris-HCl, and 1 mM EDTA, pH 7.5) and layered on 1.0 M and 1.5 M sucrose gradient and centrifuged at 60,000 g for 20 min using SW28 rotor (Beckman). Purified mitochondrial fraction was collected between 1.0 M and 1.5 M sucrose layer. Mitochondria was further washed with 5 mM Tris-HCl with 1.0 mM EDTA at 10,000 g for 15 min to collect pure mitochondria for immunoblotting [24].

Statistical analyses: Data were analyzed using R Studio

(V1.4.1717). The effects of genotype, time, and interaction between genotype and time were analyzed by employing a linear model (Variable ~ Genotype + Time + Genotype: Time) followed by Tukey's multiple comparison test. For pair-wise comparison, we employed unpaired *t*-test. No data points were excluded for analyses unless any of the samples failed in the required initial quality control assessment. For all analyses, the sample size (n) refers to cells from individual animals. In case of technical replicates, mean values were computed from the technical replicates and used for further statistical analyses. Details of the statistical treatment of the data, including pair-wise comparisons, are provided as part of the supplementary material (Tables ST1, ST3-ST5).

3. Results

3.1. Sterile inflammation alters the gene and protein level expression of selenoproteins

Reduced levels of circulating selenoprotein P (SELENOP) and total selenium in sepsis patients [25] could limit the selenium availability during acute inflammation to impact cellular response to inflammation [reviewed in 5]. We previously demonstrated that SELENOW, a highly selenium responsive protein, was one of the most abundantly expressed selenoproteins in inflamed BMDMs, implicating its plausible association in the inflammatory pathways [13]. Although the steady-state levels of selenoprotein genes and proteins have been reported earlier [12], we examined their temporal changes during the progression of inflammation, which remains largely unknown. In addition, we also examined if loss of *Selenow* altered the trait of selenium utilization for the biosynthesis of selenoproteins. RNA-seq data from WT and *Selenow*^{-/-} BMDMs sampled at 0, 4, 8, and 24 h post LPS treatment indicated no detectable expression *Dio1*, *Dio3*, *Gpx2*, *Gpx6*, and *SelenoV* in BMDMs (data not shown). However, expression of 18 other selenoproteins genes, except for *Sephs2*, indicated significant effect of time on the expression of all the selenoproteins genes, suggesting inflammation being the major determinant of changes in their expression (Fig. 2A). Directionality-based temporal changes in gene expression analyses allowed us to profile selenoproteins as part of four groups. The first group comprising of *Gpx1*, *Gpx4*, *Txnrd2*, *Selenoi*, and *Selenon* exhibited significant downregulation in their expression during the early phase (4–8 h) of inflammation, followed by their recovery to the baseline levels. *Txnrd1*, *Selenot*, *Selenos*, and *Selenof* comprised the second group characterized by a rapid increase in their expression during the early phase of acute inflammation. Except for *Selenos* and *Selenot*, expression of other two selenoproteins returned to their baseline. The expression of *Selenos* and *Selenot* remained higher at 24 h in both WT and *Selenow*^{-/-} BMDMs compared to the untreated counterparts. The third group consisted of *Gpx3*, *Selenop*, *Selenoh*, and *Selenom*. Their expression levels reduced over time with the lowest levels found at 24 h. The diminished expression of *Selenop* at 24 h was the most notable one with almost 16-fold reduction in its expression in both the genotypes when compared to the untreated control. The last group consisted of *Selenoo*, *Msrb1*, *Dio2*, *Selenok*, and *Txnrd3*. No specific trend in their expression was observed except that the levels of *Txnrd3* was significantly lower (~63% in both the genotypes) at 8 h when compared to the untreated control. Analyses of the effect of genotype (denoted as GE) indicated significant downregulation of *Selenon*, *Selenoi*, and *Dio2* involving loss of *Selenow* (Fig. 2A). The expression of *Selenoi* was always lower in the *Selenow* KO BMDMs at all time points (Table ST1). Overall, RNA-seq data indicated global downregulation of selenoprotein expression during acute inflammation in a time-dependent manner following stimulation by LPS.

We next interrogated whether the observed transcriptomic changes in selenoprotein expression were also reflected in their protein expression. LPS-induced acute inflammation had no effect on MSR1, SELENOK, and TXNRD2 protein expression in both WT and *Selenow*^{-/-} BMDMs (Fig. 2B and C). However, we found consistently higher

expression of GPX1, GPX4, TXNRD1, SELENOM, and SELENON in *Selenow*^{-/-} BMDMs compared to their WT counterparts. Specifically, increased expression (1.95 fold) of TXNRD1 was notable during the late phase (24 h) of LPS-induced inflammation in the *Selenow*^{-/-} BMDMs. We also observed a statistically non-significant increase in the intracellular expression of SELENOP in *Selenow*^{-/-} BMDMs at 2 and 24 h post-LPS stimulation (Fig. 2B). Such changes in the expression of selenoproteins, particularly the upregulation of a few selenoproteins, prompted us to further investigate the upstream pathway of selenoprotein synthesis.

3.2. Impact of inflammation on selenoprotein biosynthesis machinery

We tested the hypothesis that the observed changes in selenoprotein expression were associated with an altered expression of genes implicated in selenoprotein biosynthesis (Fig. 3A). Significant changes were noted in the expression of selenoprotein synthesis pathway genes in a time-dependent manner (Fig. 3B, Table ST1). The early phase (4 h) of acute inflammation in BMDMs involved the downregulation of *Scly*, *Sephs2*, *Sars*, and *Sars2*, even under selenium-repleted conditions. Late phase of LPS stimulation showed significant increase in *Secisbp2* and *Secisbp2l* expression. Genotype effect analyses revealed that the loss of *Selenow* impacted the expression of *Scly*, *Sephs2*, *Sars*, *Ncl*, *Rpl30*, and *Secisbp2l*. Notably, the expression of *SEPHS2* was higher in the *Selenow*^{-/-} BMDMs compared to the wild-type cells (Fig. 3C) during the late phase of inflammation, further suggesting a novel hierarchical regulation in the synthesis of select few selenoproteins in BMDMs lacking *Selenow*. Overall, these results indicated that acute inflammation also impacted the expression of selenoprotein biosynthesis machinery genes.

3.3. Dysregulated redox equilibrium in *Selenow*^{-/-} BMDMs

As mentioned earlier, *Selenow*^{-/-} BMDMs exhibited higher expression of TXNRD1, GPX1, and GPX4 at 8 and 24 h. Given that SELENOW itself exhibits disulfide and peroxide reductase activity [14], we postulated that lack of *Selenow* may lead to an oxidizing intracellular redox tone specifically under acute inflammatory conditions. To test this hypothesis, reactive oxygen species (ROS) were measured using a flow cytometry-based assay with CellRox reagent. Higher frequency of ROS-positive cells in the unstimulated *Selenow*^{-/-} BMDMs were noted. This trend persisted during the early phase of inflammation and the calculated area under the curve (AUC) was higher (~1.1 fold) in the *Selenow*^{-/-} BMDMs compared to its normal WT counterpart, implying higher ROS levels in the *Selenow*^{-/-} BMDMs post LPS stimulation (Fig. 4A and B).

3.4. Inflammatory response in *Selenow*^{-/-} bone marrow-derived macrophages

Next, we interrogated whether the absence of SELENOW impacted the inflammatory response in BMDMs following stimulation with LPS. For comprehensive analyses of all the genes that are impacted during inflammation, we mapped the expression of an expansive list of macrophage-specific human [26] and murine [27] genes (total of 385 genes) that were differentially expressed during inflammation (Table ST2). Using this inclusive and unbiased approach, we identified nine differentially expressed genes while accounting for inter-species variability in a time- and genotype-dependent manner. In *Selenow*^{-/-} BMDMs, significantly upregulated genes included *Sik1*, *Trem2*, *Ggct*, *Aif1*, and *Tlr-2*; while the downregulated genes were *Fah*, *Aqp9*, *Plk2*, and *Pmaip1* (Fig. 5A, Supplementary Fig. S1). The statistical significance and pair-wise comparison are tabulated in Table ST4. Next, we examined the expression of FAH, SIK1, SIK2, and ARG1. Although *Arg1* mRNA expression was not different in any of the time points (Fig. 5A), the protein expression of ARG1 was consistently lower in *Selenow*^{-/-} BMDMs at all time points post-LPS stimulation (Fig. 5B and C).

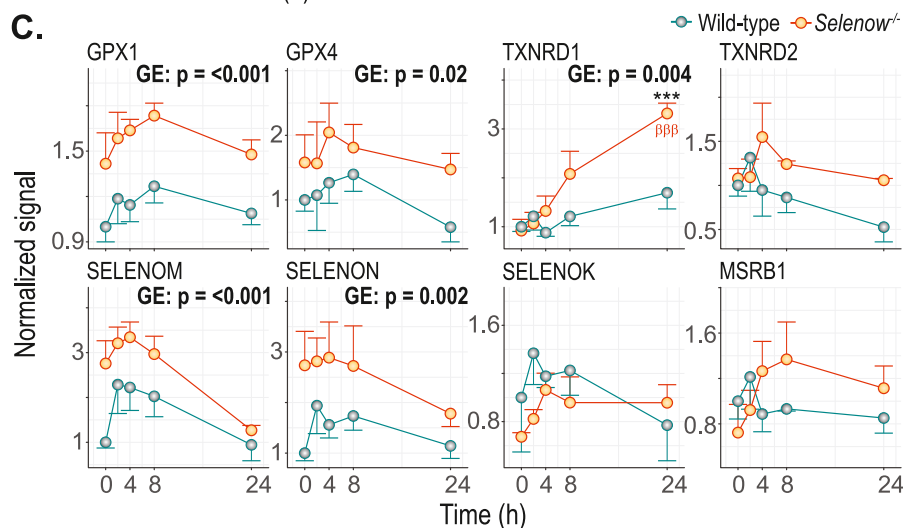
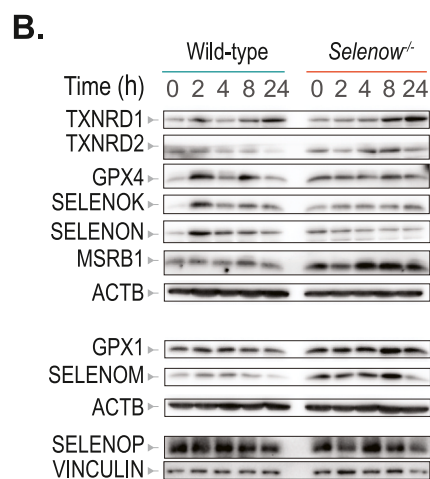
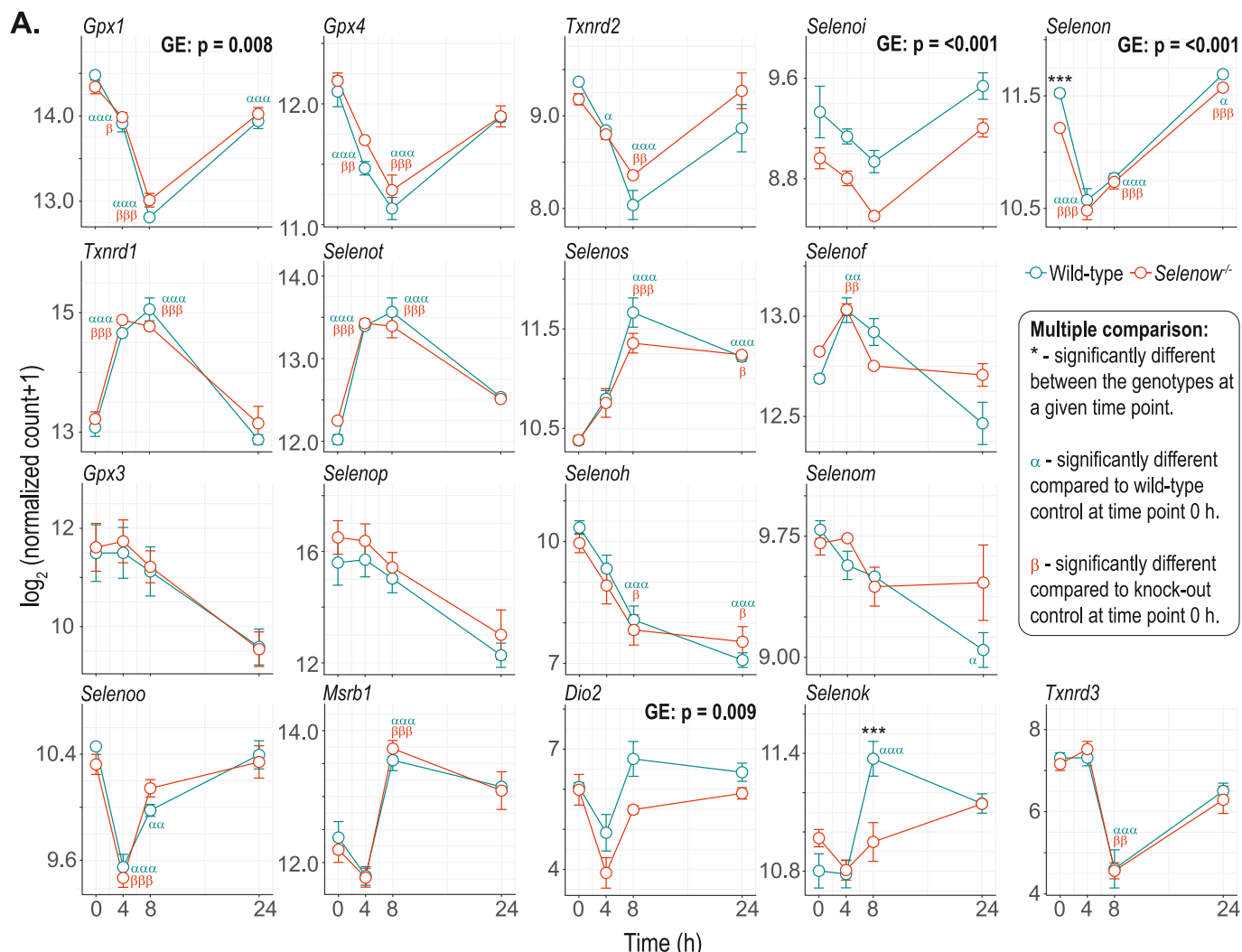


Fig. 2. A. Expression (RNAseq, normalized count data) of 18 selenoprotein genes in WT and *Selenow*^{-/-} BMDMs following treatment with 100 ng/ml LPS (n = 3 for each condition, except for KO 24 h for which only 2 replicates were available for analyses). Using the Dseq2 pipeline, the normalized expression data from RNA-seq experiment were extracted and plotted. Statistical significance was computed using a linear model, as described in the Materials and Methods section. Data have been presented as mean ± standard error of mean (SEM). GE indicates ‘genotype effect’ from two-way ANOVA analysis and the values indicates corresponding statistical significance. Mean values with asterisks (*) indicates statistically significant difference between WT and *Selenow*^{-/-} BMDMs at a given time point. Alpha (α) and beta (β) indicate statistically significant difference between time point 0 h and other time points of a measured variable in WT and *Selenow*^{-/-}, respectively. Denoted p values are as follows: */α/β = ≤0.05; **/αα/ββ = ≤0.01; ***/ααα/βββ = ≤0.001. Identical notations of statistical significance have been used throughout the manuscript. B. Representative immunoblots of selected selenoproteins in WT and *Selenow*^{-/-} BMDMs following treatment with 100 ng/ml LPS (n = 3). C. Semi-quantitative analyses of selenoprotein expression as outlined above. Band intensity was measured using Image J software (n = 3).

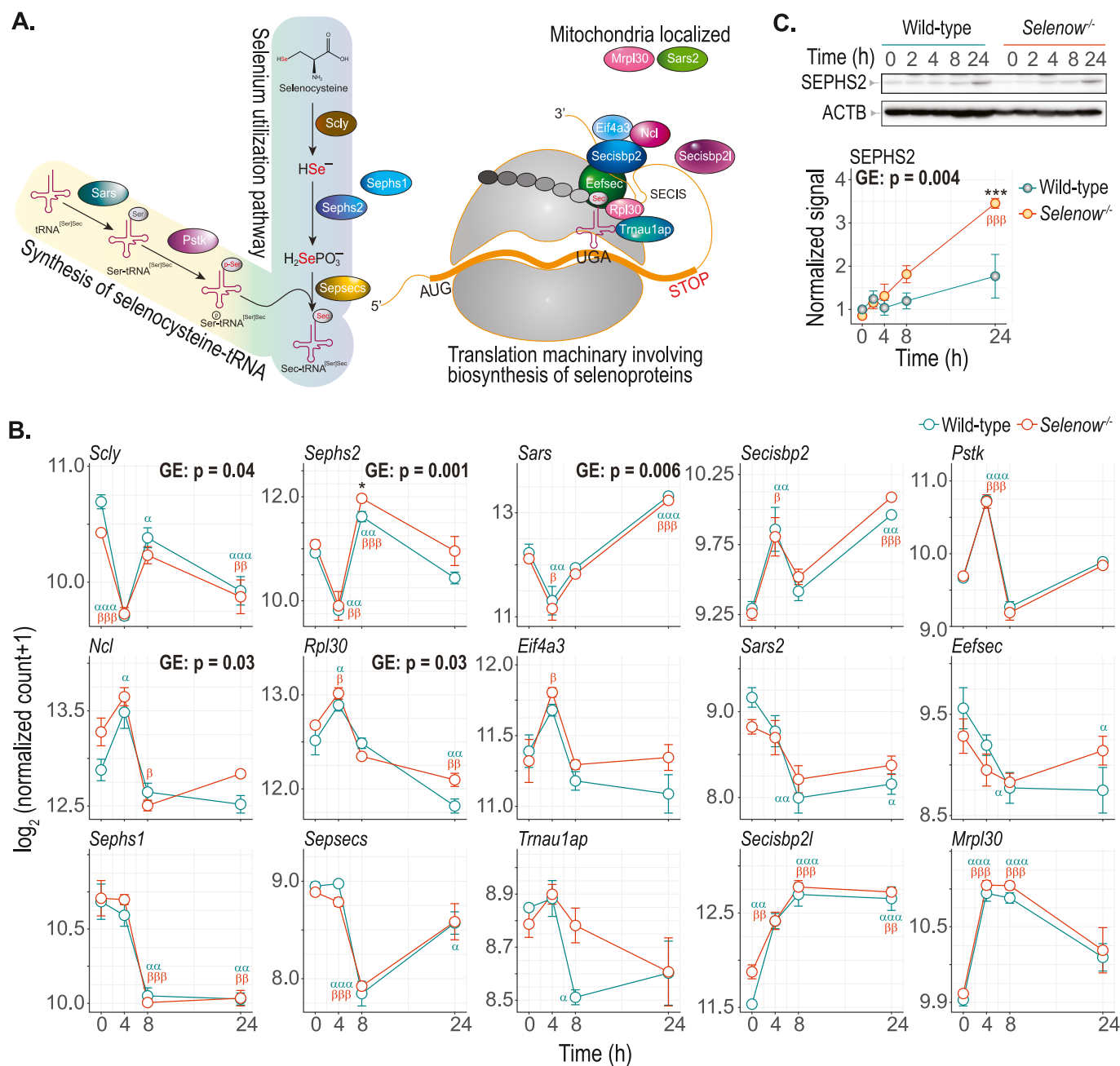


Fig. 3. A. A schematic diagram describing the pathway involved in the biogenesis of selenoproteins mRNAs and subsequent translation of mRNAs into nascent polypeptides of selenoproteins. B. Expression (RNAseq, normalized count data) of 15 genes that are associated with the biosynthesis of selenoproteins in WT and *Selenow*^{-/-} BMDMs following treatment with 100 ng/ml LPS. Although, the involvement of *Sephs1* in selenoproteins biosynthesis is not well-characterized, we also probed its expression during sterile inflammation. For the details on the statistical analyses, please refer to Fig. 2A legend. C. Top panel, Immunoblot of SEPHS2 from whole-cell lysate of WT and *Selenow*^{-/-} BMDMs following treatment with 100 ng/ml LPS (n = 3). Bottom panel, Semi-quantitative analyses of SEPHS2 expression.

Corroborating with the transcript data, the expression of FAH, the last enzyme in the catabolic pathway of tyrosine, was also significantly lower in *Selenow*^{-/-} BMDMs. Similarly, *Selenow*^{-/-} BMDMs exhibited significantly lower expression of SIK1. Interestingly, the loss of *Selenow* resulted in higher expression of SIK2, an isoform of the salt-inducible subfamily of AMPK family of kinases implicated in the regulation of multiple cellular pathways, including 14-3-3 signaling ((Fig. 5B and C).

Reduced ARG1 and FAH in *Selenow*^{-/-} BMDMs prompted us to probe the arginine metabolism pathway (Fig. 5D). We queried the total levels of intermediate metabolites of arginine that were detected by targeted metabolomics. We found that ornithine and citrulline were significantly lower in the *Selenow*^{-/-} BMDMs at 24 h (Fig. 5E). The ratio of ornithine/

arginine and citrulline/arginine were also significantly lower in *Selenow*^{-/-} BMDMs (Fig. 5F). Taken together, these results suggested impaired arginine metabolism in *Selenow*^{-/-} BMDMs at later time points (>8 h).

To examine whether reduced expression of ARG1 in *Selenow*^{-/-} BMDMs has functional consequences on the engulfment of apoptotic or dead cells, we performed an efferocytosis assay with PKH26 labeled neutrophils. Increased frequency of PKH26⁺F4/80⁺ WT BMDMs compared to *Selenow*^{-/-} BMDMs (Fig. 5G) indicated limited clearance capacity of dead/apoptotic cells in BMDMs that lacked SELENOW. These results suggest that the loss of SELENOW might impact resolution of inflammation, possibly linked to reduced expression of ARG1 leading to

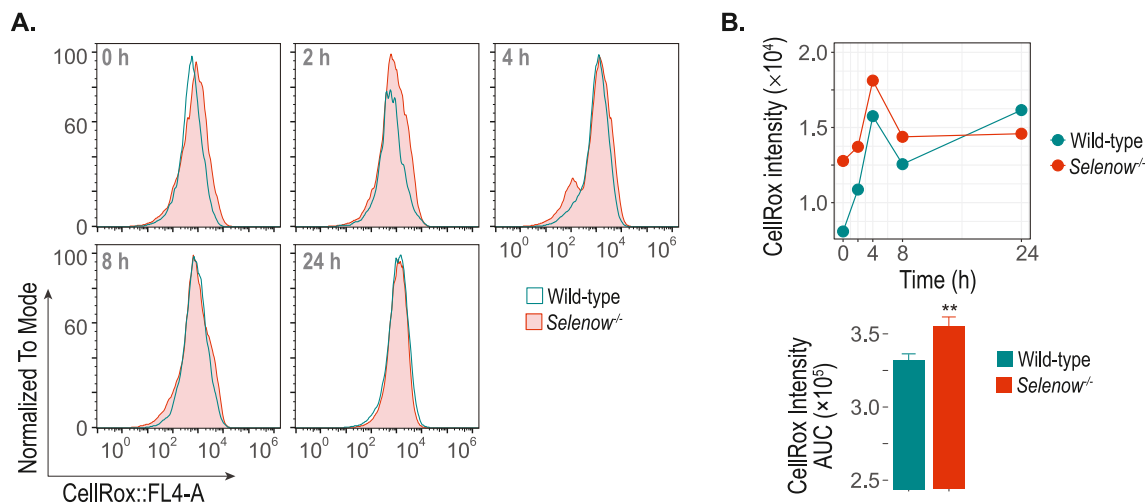


Fig. 4. A. Flow cytometry analysis of the frequency of ROS-positive cells in WT and *Selenow*^{-/-} BMDMs following treatment with LPS (100 ng/ml). Data from 3 independent experiments were concatenated and presented as is. Histograms demonstrate the relative frequency of ROS-positive viable cells (n = 3). B. Median CellRox ROS intensity of WT and *Selenow*^{-/-} BMDMs (top panel) and the area under the curve (bottom panel) of ROS intensity from the same experiments, as outlined above (n = 3). SEM values were not calculated for CellRox ROS intensity data as samples were concatenated for analyses. Statistical significance of AUC for ROS intensity was computed using unpaired *t*-test.

significantly lower levels of ornithine.

3.5. Loss of *Selenow* impacts cellular respiration

Increased ROS levels in *Selenow*^{-/-} BMDMs suggested plausible involvement of one or more cellular processes implicated in ROS generation. Loss of electron from the electron transport chain involving mitochondrial respiration is one such established pathway. In a time-course study, we examined oxygen consumption rate (OCR) in BMDMs at basal condition and upon stimulation with LPS. *Selenow*^{-/-} BMDMs exhibited higher basal respiration at all time point (Fig. 6A and C). Metabolic switching from oxidative phosphorylation to glycolysis is a hallmark of adaptive metabolic response in macrophages upon inflammation [28]. Metabolic phenotype profiling using mitochondrial stress test assay demonstrated a progressive switch towards glycolytic phenotype in BMDMs originated from both genotypes (Fig. 6B) but with a distinct signature. Oligomycin-induced inhibition of ATP-synthase resulted in characteristic reduction of OCR that were not different between the genotypes. However, FCCP-induced uncoupling of mitochondrial membrane potential resulted in increased oxygen consumption rate in *Selenow*^{-/-} BMDMs when compared to their WT counterparts, as reflected by significant increase in maximal respiration in a genotype-dependent manner (Fig. 6C). An apparent increase in the uncoupling activity was noted in *Selenow*^{-/-} BMDMs as demonstrated by significantly higher proton leak. Despite this, higher ATP production was always seen in *Selenow*^{-/-} BMDMs prior to LPS stimulation and post LPS-stimulation (Fig. 6C).

Metabolic phenotype profiling data suggested that *Selenow*^{-/-} BMDMs might lack the capacity to enhance glycolytic metabolism (Fig. 6B), as observed during acute inflammation. Temporal changes in OCR and ECAR ratio (extracellular acidification rate) for qualitative assessment of the relative utilization of mitochondrial (oxidative) versus glycolytic pathways for energy production was examined (Fig. 7A). Comparison of the shift in the OCR/ECAR ratio between 4 and 8 h indicated a significant increase in this value only in the wild-type BMDMs, which necessitated a glycolytic stress test. The rate of glycolysis (ECAR) was similar between the BMDMs isolated from both the genotypes at baseline (Fig. 7B and C). Following LPS stimulation for 4 and 8 h, the glycolytic respiration was higher in the WT BMDMs compared to those isolated from the *Selenow*^{-/-} mice (Fig. 7B). In line with this, distinct effects of genotype were observed for glycolysis (p =

0.003), non-glycolytic acidification (p = 0.01), glycolytic capacity (p = 0.003), and glycolytic reserve (p = 0.015) (Fig. 7C). All of these measurements were lower in the *Selenow*^{-/-} BMDMs when compared to their WT counterparts, suggesting plausible involvement of SELENOW in inflammation-associated metabolic reprogramming. To explore if the observed differences in glycolysis between the genotypes could be attributed to the differential expression of glucose transporters that may limit glucose availability, we examined the expression of key glucose transporters from the RNA-seq data. However, no significant differences in their mRNA expression were noted (Supplementary Fig. 2).

3.6. Altered glycolysis, TCA cycle, and thiol redox homeostasis in *Selenow*^{-/-} BMDMs

Mitochondrial and glycolytic stress tests indicated a clear difference in glucose utilization pathway between WT and *Selenow*^{-/-} BMDMs. To address this, we measured glycolytic and TCA cycle flux using [U-¹³C] glucose (Fig. 8A). The relative abundance of ¹³C₆-labeled and unlabeled glucose was similar between the genotypes at all time points, suggesting uniform isotopic enrichment of labeled glucose (Fig. 8B). The levels of pyruvate and lactate were lower in the *Selenow*^{-/-} BMDMs (Fig. 8C). Specifically, the levels of lactate were significantly lower at 24 h, corroborating to the findings from the glycolytic stress test assay that demonstrated impaired glycolytic metabolism in macrophages lacking SELENOW. We also observed reduced levels of TCA cycle intermediates citrate/isocitrate, fumarate, and malate in the *Selenow*^{-/-} BMDMs (Fig. 8D). Furthermore, acute inflammation led to a progressive increase in GSH levels and GSH: GSSG ratio in both the phenotypes, which corroborated with higher ROS levels in these cells.

3.7. *Selenow* is a mitochondrial-resident protein

Selenow^{-/-} BMDMs exhibited higher basal mitochondrial respiration even in the absence of LPS stimulation. Furthermore, glycolytic stress test suggested that the ablation of *Selenow* impaired the characteristic increase in inflammation-associated glycolysis. We speculated that SELENOW could also be localized to the mitochondria despite existing public databases suggesting it to be a cytosolic protein. Unprocessed SELENOW polypeptide lacks a canonical mitochondrial localizing signal peptide, which was also corroborated by bioinformatics-based neural network analysis using DeepMito (<http://busca.biocomp.unibo.it/deep>

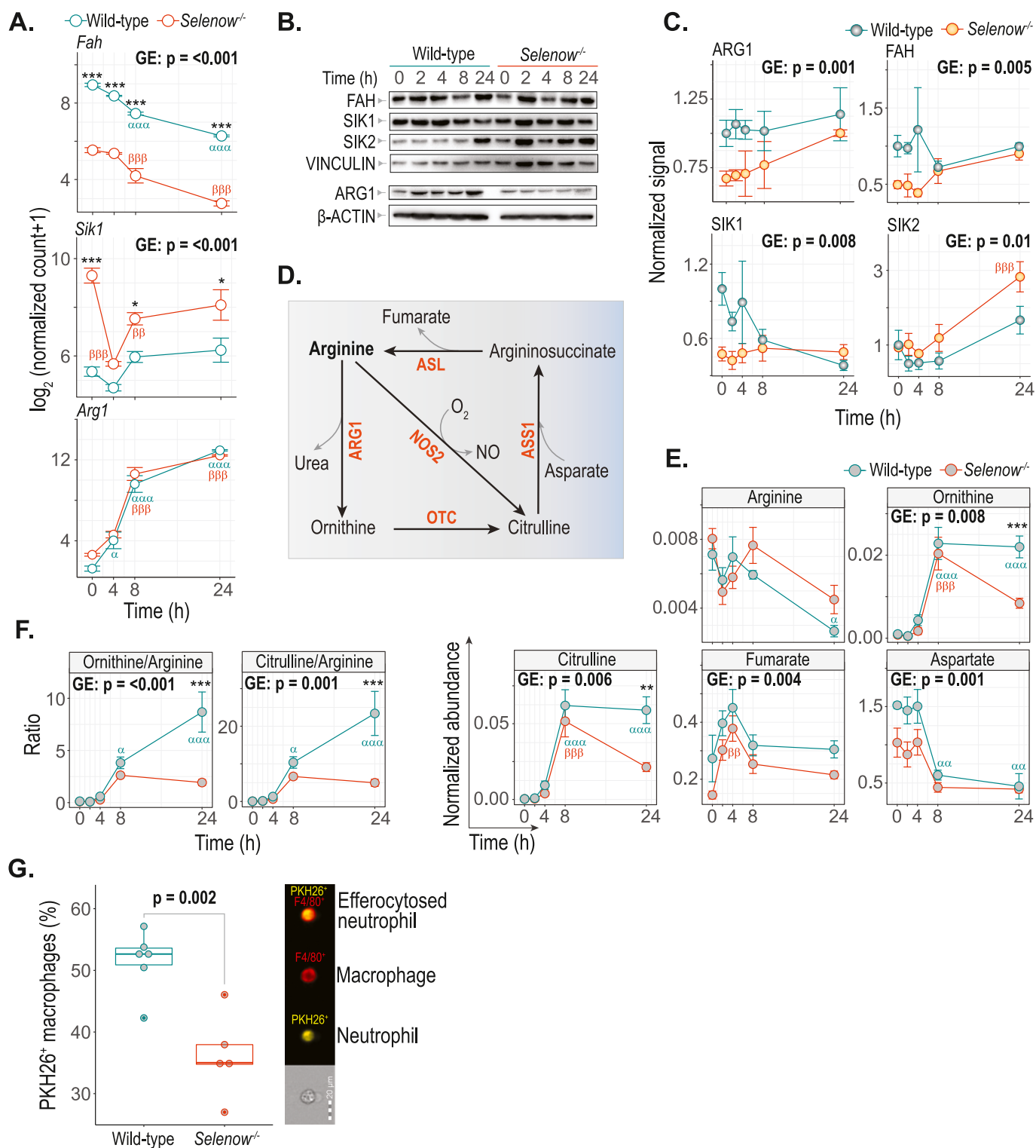


Fig. 5. **A.** Temporal changes in the expression of selected genes of inflammatory pathway that were differentially expressed between WT and *Selenow*^{-/-} BMDMs following treatment with 100 ng/ml LPS. Detailed multiple comparisons between the groups from two-way ANOVA are summarized in the Supplementary Table ST1. For the details on the statistical analyses, please refer to Fig. 2A legend. **B and C.** Representative immunoblots and semi-quantitative analyses of FAH, SIK1, SIK2, and ARG1 expression in BMDMs lysates (n = 3). **D.** Schematic representation of pathway involved in arginine metabolism. **E.** Normalized abundance of arginine, ornithine, citrulline, fumarate, and aspartate in WT and *Selenow*^{-/-} BMDMs following treatment with LPS (n = 3). **F.** Ornithine to arginine and citrulline to arginine ratio in WT and *Selenow*^{-/-} BMDMs. For the details on the statistical analyses, please refer to Fig. 2A legend (n = 3). **G. Left panel,** Efferocytosis in WT and *Selenow*^{-/-} BMDMs macrophages that were co-cultured with PKH26-stained apoptotic/dying neutrophils for 4 h without any stimulation. Statistical significance was computed using unpaired *t*-test (n = 3). **Right panel,** Representative flow sight image demonstrating a macrophage that engulfed a PKH26-labeled neutrophil via efferocytosis.

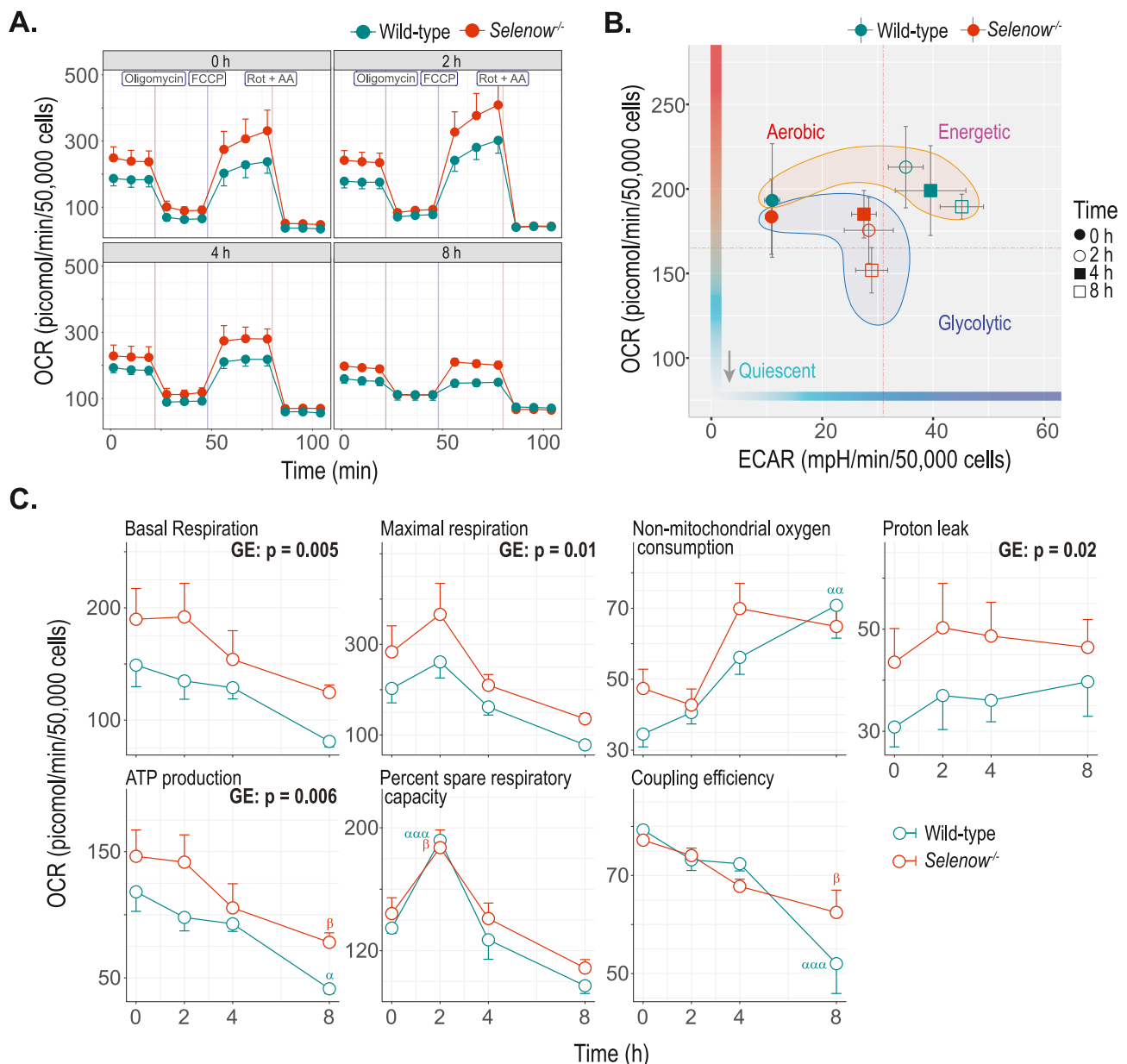


Fig. 6. A. A real-time recording of oxygen consumption rates (OCR) in WT and *Selenow*^{-/-} BMDMs following treatment with 100 ng/ml LPS (n = 5) for 1 h followed by sampling at the indicated time points (n = 5). *Abbreviation*, FCCP – Carbonyl cyanide-4 (trifluoromethoxy) phenylhydrazone, Rot – Rotenone, AA - antimycin A. **B.** Metabolic phenotypes of BMDMs as computed from data obtained from the mitochondrial stress test, as described in Fig. 6A. **C.** The calculated values for basal respiration, maximal respiration, non-mitochondrial respiration, proton leak, ATP production, percent spare respiratory capacity, and coupling efficiency from the mitochondrial stress test (n = 5). For the details on the statistical analyses, please refer to Fig. 2A legend.

mito/) prediction tool. Regardless, immunoblotting analysis of cytosolic and mitochondrial fractions from murine liver lysates showed the presence of SELENOW along with VDAC, a mitochondria-resident protein (Fig. 9A). The purity of the mitochondrial fraction was confirmed by the absence of any immunoreactivity towards GAPDH and Histone H3. Co-localization of mitochondria-resident cytochrome oxidase 4 (COX4) with SELENOW was further confirmed in WT BMDMs using super-resolution fluorescence microscopy (VT-iSIM, BioVision) (Fig. 9B). Taken together, these studies confirm the localization of SELENOW to mitochondria and cytosol.

4. Discussion

Recent studies have demonstrated the role of SELENOW as a disulfide and peroxide reductase in addition to its ability to modulate diverse

cell signaling pathways, via its interaction with cellular proteins, including 14-3-3 proteins [14,15,29]. Interestingly, the onset of inflammation severely impacts the selenium utilization pathway both at cellular and systemic levels, which is corroborated by the loss of total selenium and selenoprotein P during severe inflammation, as in septic shock [25,30–32]. To dissect the role of SELENOW, a highly expressed selenoprotein in macrophages during LPS-induced inflammation, this study interrogated temporal changes in the selenium utilization and selenoprotein biosynthetic pathways in BMDMs under adequate selenium availability. Loss of SELENOW in BMDMs impacted the expression of several key selenoproteins during LPS-induced acute inflammation, which was associated with augmented mitochondrial respiration, increased oxidative stress, and a disrupted canonical metabolic switching involving glycolysis and OXPHOS.

Our study demonstrated that acute inflammation conferred unique

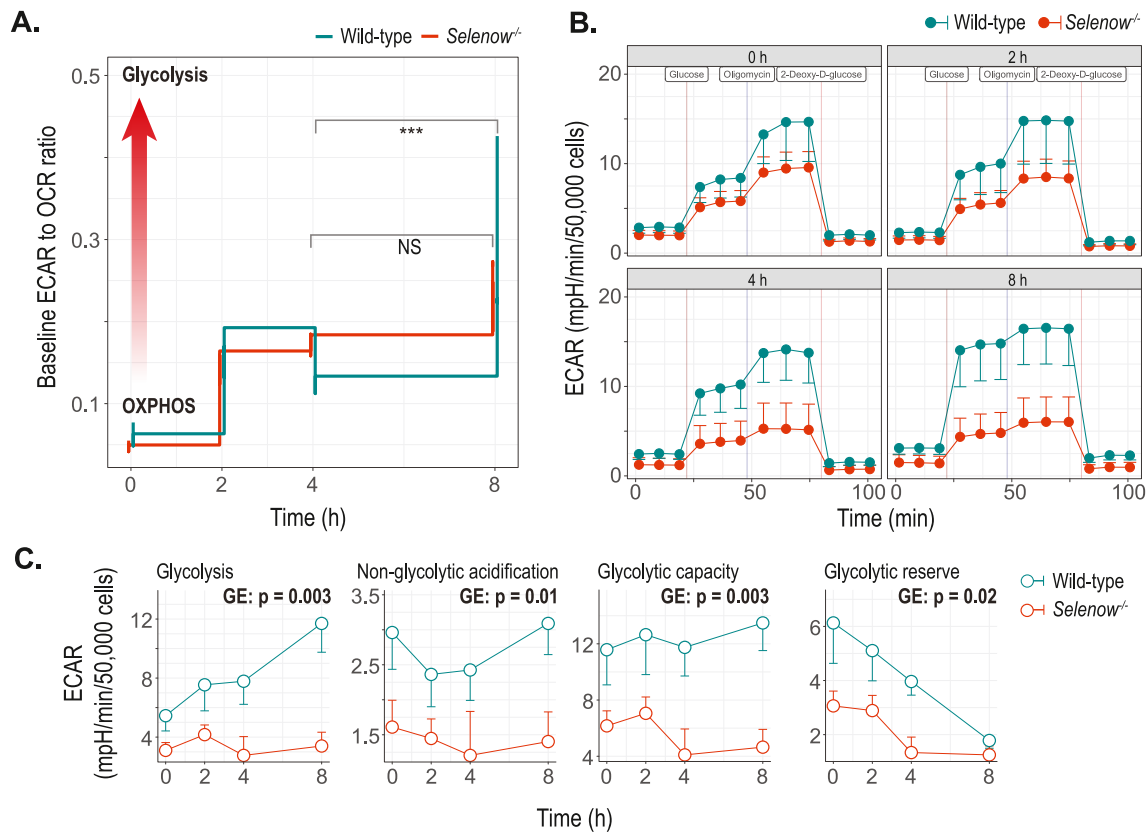


Fig. 7. A. Qualitative assessment of the relative utilization of mitochondrial (oxidative phosphorylation) versus glycolytic pathways for energy production. OCR and extracellular acidification rates (ECAR) data are obtained from the glycolytic stress test, as outlined in Fig. 6A. B. Extracellular acidification rates in WT and *Selenow*^{-/-} BMDMs following treatment with 100 ng/ml LPS (n = 3) for 1 h followed by sampling at the indicated time points (n = 3). C. The rate of glycolysis (top left), non-glycolytic acidification (top right), glycolytic capacity (bottom left), and glycolytic reserve (bottom right) measured from the outlined glycolytic stress test (n = 3). For the details on the statistical analyses, please refer to Fig. 2A legend.

selectivity in the transcription of selenoprotein genes. Overall, these findings indicated a discordance between transcription and translation of selenoprotein genes in macrophages during acute inflammation even under adequate selenium availability. Such anomalies culminate in overall disruption of homeostasis of selenoprotein biosynthesis. It remains to be understood whether such changes in selenoprotein expression are essential for mounting optimal inflammatory response. In our study, we did not find any notable differences in the selenoprotein gene expression associated with the loss of *Selenow*. However, the expression of several selenoproteins (GPX1, GPX4, and TXNRD1) were significantly higher in the *Selenow*^{-/-} BMDMs compared to their WT counterparts, which indicates a possible compensatory effect. The mechanistic basis for the above observation remains to be elucidated, specifically when selenium availability is not a limiting factor.

Selenow^{-/-} BMDMs exhibited higher basal ROS level compared to their WT counterparts. Exposure to LPS further exacerbated the ROS levels, suggesting the importance of peroxidase activity of SELENOW. These findings also imply that inflammation-associated increase in ROS may alter the dynamics of selenium utilization traits. During inflammation where ROS is consistently produced, the hierarchy of certain selenoproteins is important to maintain the cellular peroxide tone, which is key to regulating upstream signaling events. Our findings corroborate with previously reported effects in *Trsp* knock-out peritoneal [33] and bone marrow-derived macrophages [12] that exhibited higher basal ROS levels in the absence of inflammatory stimuli.

In this study, we found increased expression of *Ggct* and *Sik1* among five upregulated genes in *Selenow*^{-/-} BMDMs. However, protein level expression of SIK1 was lower in *Selenow*^{-/-} BMDMs upon LPS stimulation, suggesting a post-transcriptional regulation of this serine/

threonine kinase. Interestingly, murine BMDMs overexpressing the kinase domain deficient SIK2 exhibited an anti-inflammatory (M2) phenotype characterized by an increased expression of ARG1 [34]. Similarly, chemical inhibition of SIK2 also resulted in an anti-inflammatory phenotype. This is in close agreement with our data where increased levels of SIK2 expression in *Selenow*^{-/-} BMDMs was associated with significantly lower ARG1 expression accompanied by decreased levels of ornithine upon LPS treatment. Specifically reduced expression of ARG1 might have direct implications on the phagocytic activity of macrophages given that the deficiency of *Arg1* in macrophages has been implicated in compromised efferocytosis [35]. In our study, we also noted limited phagocytic activity of *Selenow*^{-/-} BMDMs towards neutrophils as demonstrated in the efferocytosis assay. A recent study demonstrated the interaction between SELENOW with arginine-tRNA ligase (RARS) and argininosuccinate synthase (ASS1), thereby linking the plausible role of this selenoprotein in multiple nodal points in arginine metabolism and mRNA translation [29]. Taken together, these data support the notion that *Selenow*^{-/-} BMDMs exhibit a unique phenotype that appears to be defective in the resolution of inflammation. This is currently being investigated in our laboratory and will be reported in the future.

In this study, we found remarkable reduction of *Fah* expression coupled with lower levels of fumarate suggesting an altered tyrosine catabolism in *Selenow*^{-/-} BMDMs. Decreased levels of fumarate is also reminiscent of a disrupted TCA cycle as previously reported in selenium deficient BMDMs, where no selenoproteins, including SELENOW, were expressed [13,36]. Inhibition of succinate dehydrogenase (SDH-A) with dimethylmalonate in mice maintained on selenium replete diets increased the time for resolution in a model of peritonitis indicating that

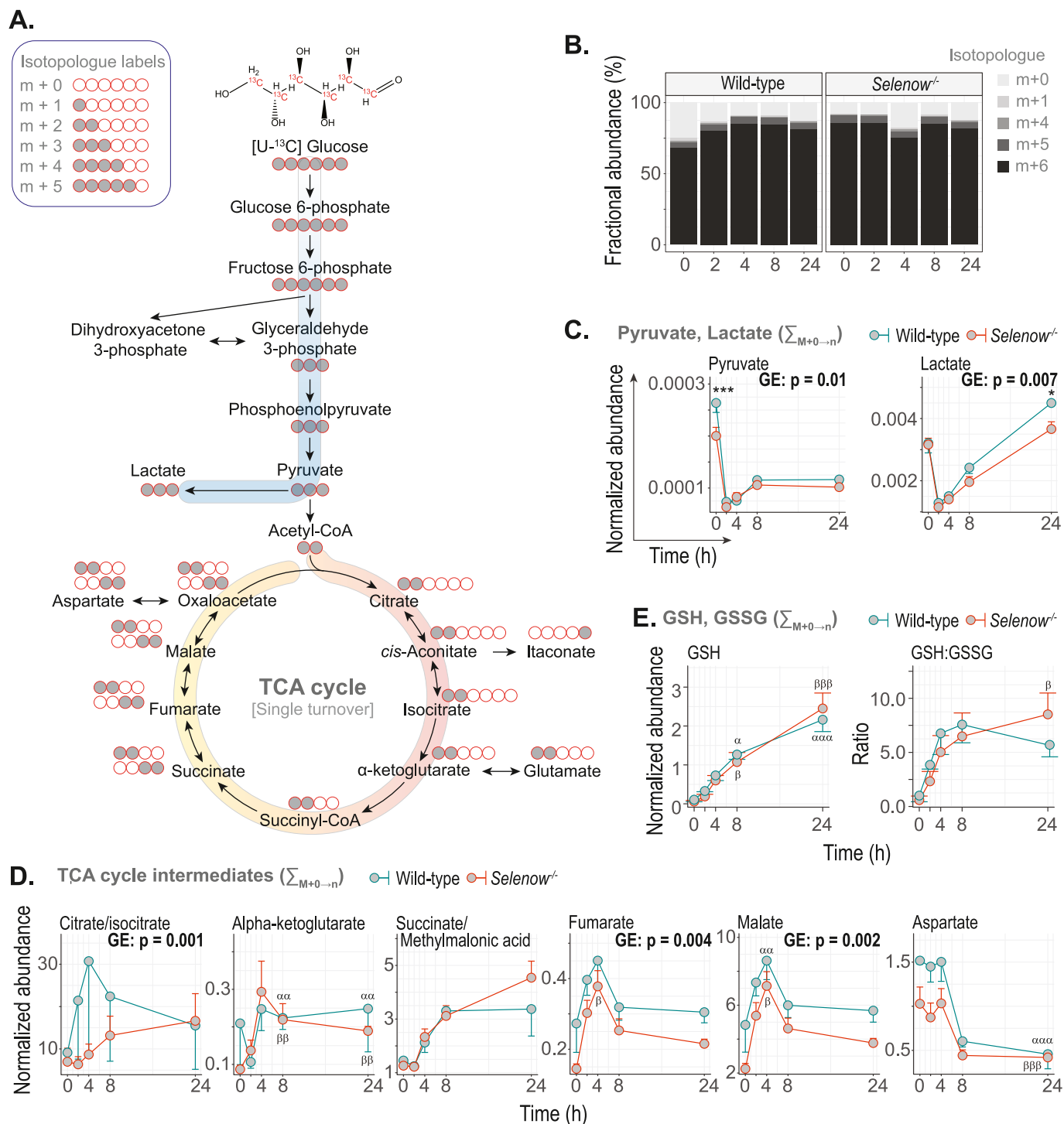


Fig. 8. **A.** A schematic demonstrating the metabolic flux of isotope-enriched carbon from U-¹³C-glucose involving glycolysis and TCA cycle. Isotopologue signatures from single cycle turnover of glucose into lactate via glycolysis or into oxaloacetate via TCA cycle are shown next to the corresponding metabolite. **B.** Distribution of unlabeled and U-¹³C-labeled glucose at different time points. No significant differences in the labeling indices were observed at any time point or between the genotypes (n = 3). **C.** The levels of pyruvate and lactate (sum of all isotopologue) in WT and *Selenow*^{-/-} BMDMs following treatment with LPS for the indicated time points (n = 3). **D.** The normalized abundance of selected TCA cycle intermediates and aspartate in WT and *Selenow*^{-/-} BMDMs following treatment with LPS. Sum of all isotopologue were used to calculate the normalized abundance (n = 3). For the details on the statistical analyses, please refer to Fig. 2A legend. **E.** The levels of GSH and GSH to GSSG ratio in WT and *Selenow*^{-/-} BMDMs following treatment with LPS (n = 3).

decreased fumarate is a sign of disrupted metabolism and resolution [13]. Together, these results imply that SELENOW may play a role in arginine and tyrosine metabolism.

A key finding in our study was atypical metabolic phenotype switching of *Selenow*^{-/-} BMDMs. In general, pro-inflammatory

macrophages exhibit higher rates of glycolysis, whereas oxidative phosphorylation serves as the main energy source for pro-resolving macrophages [28]. In this study, *Selenow*^{-/-} BMDMs exhibited increased mitochondrial respiration and lacked the capacity to increase glycolysis upon induction of acute inflammation that was corroborated

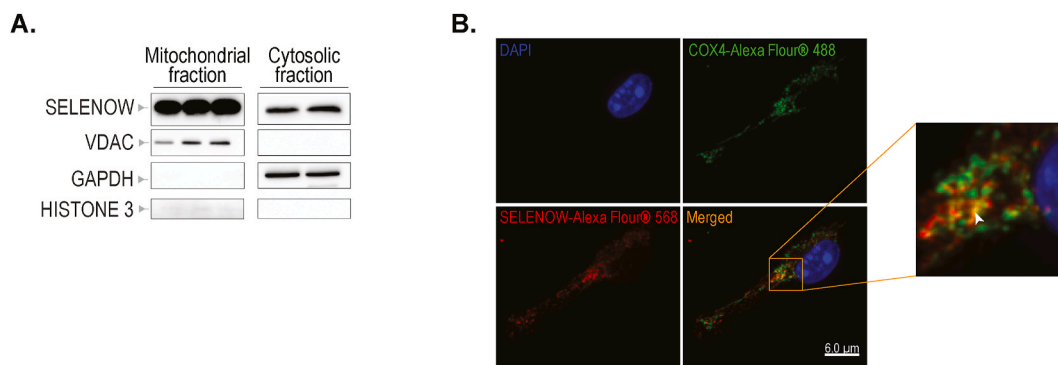


Fig. 9. A. Immunoblot analysis of SELENOW in lysates prepared from the isolated mitochondrial fraction of whole liver of WT mice. VDAC, GAPDH, and histone 3 served as control for mitochondrial, cytosolic, and nuclear localization, respectively. B. Immunofluorescence detection of SELENOW in WT BMDMs. Merged signal in orange pseudo-color depicts colocalization of SELENOW along with COX4 in the mitochondria, as illustrated in the inset with white arrow. Scale bar = 6 μm . (For interpretation of the references to color in this figure legend, the reader is referred to the Web version of this article.)

by decreased levels of intracellular lactate at later time points. Furthermore, over time post LPS treatment, *Selenow*^{-/-} BMDMs failed to increase glycolytic respiration, suggesting that SELENOW may play an important role in metabolic switching during the progression of early inflammation. Interactions between SELENOW with 14-3-3 and Rictor may partly explain this. Transient loss of SELENOW increases the interaction between 14-3-3 and Rictor, resulting in the decreased mTORC2-dependent phosphorylation of AKT at Ser473 [18]. It is plausible that in the absence of SELENOW, a stable interaction between 14-3-3 and Rictor could exert a negative effect on mTORC2 activation required for increased glycolysis. In line with this, Rictor-deficient murine dendritic cells rely on increased mitochondrial respiration following LPS stimulation as opposed to glycolysis [37].

Increased mitochondrial ATP production in *Selenow*^{-/-} BMDMs at baseline suggested increased energy requirement of these cells. At the same time, higher proton leak in these macrophages indicated a companion effect coupled with increased mitochondrial respiration. Corresponding lower levels of pyruvate, citrate/isocitrate, fumarate, and malate in the *Selenow*^{-/-} BMDMs suggested that the shunt to TCA cycle from glycolysis was limited. This is suggestive of two different scenarios. First, the lower levels of pyruvate in *Selenow*^{-/-} BMDMs potentially limited its turnover into TCA cycle intermediates with the possible involvement of anaplerosis from other substrates that fuels TCA cycle. Alternatively, amino acids and fatty acids were more likely preferentially utilized for energy production. The mechanisms involving such metabolic reprogramming involving loss of SELENOW in macrophages remains to be studied in the future. Some of these effects could be, in part, due to the mitochondrial localization of SELENOW which was also recently described in T cells [29]. It is plausible that SELENOW forms complexes with other proteins known to shuttle into the mitochondria to impact above pathways, which needs to be elucidated further.

In summary, we demonstrate that LPS-induced acute inflammation impacts the expression of selenoproteins and those involved in the selenoprotein biosynthetic pathway, suggesting a hierarchy in their transcriptional and translational control. Genetic ablation of *Selenow* resulted in increased ROS production, with an atypical metabolic phenotype characterized by increased mitochondrial metabolism instead of glycolysis during inflammation. Such metabolic adaptation may have consequences on the pathways of resolution of inflammation. Thus, our findings provide new insights into the role of SELENOW in inflammation and its resolution.

Data availability

RNA-seq data has been submitted to GEO with accession number GSE211683.

Conflict-of-interest statement

All the authors have read the manuscript and approved its final version before the submission. None of the authors have any potential conflict-of-interests to declare.

Acknowledgements

This study was funded, in part, by grants, DK077152 and DK0119865 from the National Institutes of Health (NIH) to KSP, USDA-NIFA Hatch project # PEN04771; accession #0000005 to KSP and SM, and # Project PEN04772 and Accession number #7000371 to ADP. MAH acknowledges support from the NIH (CA239256), USDA-NIFA Hatch project #PEN04275; accession #1018544, and the Dr. Frances Keesler Graham Early Career Professorship. We thank the Metabolomics Core Facility, Penn State Huck Institutes of the Life Sciences, Penn State Cancer Institute, and members in Prabhu laboratory for timely help and engaging discussions.

Appendix A. Supplementary data

Supplementary data to this article can be found online at <https://doi.org/10.1016/j.redox.2022.102571>.

References

- [1] B. Brune, N. Dehne, N. Grossmann, M. Jung, D. Namgaladze, T. Schmid, A. von Knethen, A. Weigert, Redox control of inflammation in macrophages, *Antioxidants Redox Signal.* 19 (6) (2013) 595–637.
- [2] H.J. Forman, H. Zhang, Targeting oxidative stress in disease: promise and limitations of antioxidant therapy, *Nat. Rev. Drug Discov.* 20 (9) (2021) 689–709.
- [3] V.M. Labunsky, D.L. Hatfield, V.N. Gladyshev, Selenoproteins: molecular pathways and physiological roles, *Physiol. Rev.* 94 (3) (2014) 739–777.
- [4] B.C. Lee, S.-G. Lee, M.-K. Choo, J.H. Kim, H.M. Lee, S. Kim, D.E. Fomenko, H.-Y. Kim, J.M. Park, V.N. Gladyshev, Selenoprotein MsrB1 promotes anti-inflammatory cytokine gene expression in macrophages and controls immune response in vivo, *Sci. Rep.* 7 (1) (2017) 5119.
- [5] F. Qian, S. Misra, K.S. Prabhu, Selenium and selenoproteins in prostanoid metabolism and immunity, *Crit. Rev. Biochem. Mol. Biol.* 54 (6) (2019) 484–516.
- [6] B.T. Diwakar, A.M. Korwar, R.F. Paulson, K.S. Prabhu, The regulation of pathways of inflammation and resolution in immune cells and cancer stem cells by selenium, *Adv. Cancer Res.* 136 (2017) 153–172.
- [7] L.H. Duntas, Selenium and inflammation: underlying anti-inflammatory mechanisms, *Hormone and metabolic research = Hormon- und Stoffwechselforschung = Hormones et métabolisme* 41 (6) (2009) 443–447.
- [8] R. Gärtner, W. Albrich, M.W. Angstwurm, The effect of a selenium supplementation on the outcome of patients with severe systemic inflammation, burn and trauma, *Biofactors* 14 (1–4) (2001) 199–204.
- [9] Z. Huang, A.H. Rose, P.R. Hoffmann, The role of selenium in inflammation and immunity: from molecular mechanisms to therapeutic opportunities, *Antioxidants Redox Signal.* 16 (7) (2012) 705–743.
- [10] D.J. Kominsky, E.L. Campbell, S.P. Colgan, Metabolic shifts in immunity and inflammation, *J. Immunol.* 184 (8) (2010) 4062–4068.

- [11] J.C. Avery, P.R. Hoffmann, Selenium, selenoproteins, and immunity, *Nutrients* 10 (9) (2018).
- [12] B.A. Carlson, M.-H. Yoo, Y. Sano, A. Sengupta, J.Y. Kim, R. Irons, V.N. Gladyshev, D.L. Hatfield, J.M. Park, Selenoproteins regulate macrophage invasiveness and extracellular matrix-related gene expression, *BMC Immunol.* 10 (1) (2009) 57.
- [13] A.M. Korwar, A. Hossain, T.J. Lee, A.E. Shay, V. Basrur, K. Conlon, P.B. Smith, B. A. Carlson, H.M. Salis, A.D. Patterson, K.S. Prabhu, Selenium-dependent metabolic reprogramming during inflammation and resolution, *J. Biol. Chem.* 296 (2021), 100410.
- [14] D.-w. Jeong, T.S. Kim, Y.W. Chung, B.J. Lee, I.Y. Kim, Selenoprotein W is a glutathione-dependent antioxidant in vivo, *FEBS (Fed. Eur. Biochem. Soc.) Lett.* 517 (1) (2002) 225–228.
- [15] Y.H. Jeon, K.Y. Ko, J.H. Lee, K.J. Park, J.K. Jang, I.Y. Kim, Identification of a redox-modulatory interaction between selenoprotein W and 14-3-3 protein, *Biochim. Biophys. Acta Mol. Cell Res.* 1863 (1) (2016) 10–18.
- [16] K.L. Pennington, T.Y. Chan, M.P. Torres, J.L. Andersen, The dynamic and stress-adaptive signaling hub of 14-3-3: emerging mechanisms of regulation and context-dependent protein–protein interactions, *Oncogene* 37 (42) (2018) 5587–5604.
- [17] C.C. Munier, C. Ottmann, M.W.D. Perry, 14-3-3 modulation of the inflammatory response, *Pharmacol. Res.* 163 (2021), 105236.
- [18] Y.H. Jeon, Y.H. Park, J.H. Kwon, J.H. Lee, I.Y. Kim, Inhibition of 14-3-3 binding to Rictor of mTORC2 for Akt phosphorylation at Ser473 is regulated by selenoprotein W, *Biochim. Biophys. Acta* 1833 (10) (2013) 2135–2142.
- [19] D.D. Sarbassov, D.A. Guertin, S.M. Ali, D.M. Sabatini, Phosphorylation and regulation of Akt/PKB by the rictor-mTOR complex, *Science* 307 (5712) (2005) 1098–1101.
- [20] A.E. Shay, B.T. Diwakar, B.-J. Guan, V. Narayan, J.F. Urban, K.S. Prabhu, IL-4 up-regulates cyclooxygenase-1 expression in macrophages, *J. Biol. Chem.* 292 (35) (2017) 14544–14555.
- [21] W. Lu, M.F. Clasquin, E. Melamud, D. Amador-Noguez, A.A. Caudy, J. D. Rabinowitz, Metabolomic analysis via reversed-phase ion-pairing liquid chromatography coupled to a stand alone orbitrap mass spectrometer, *Anal. Chem.* 82 (8) (2010) 3212–3221.
- [22] H. Tsugawa, T. Cajka, T. Kind, Y. Ma, B. Higgins, K. Ikeda, M. Kanazawa, J. VanderGheynst, O. Fiehn, M. Arita, MS-DIAL: data-independent MS/MS deconvolution for comprehensive metabolome analysis, *Nat. Methods* 12 (6) (2015) 523–526.
- [23] P.C. Liao, C. Bergamini, R. Fato, L.A. Pon, F. Pallotti, Isolation of mitochondria from cells and tissues, *Methods Cell Biol.* 155 (2020) 3–31.
- [24] D.A. Clayton, G.S. Shadel, Purification of mitochondria by sucrose step density gradient centrifugation, *Cold Spring Harb. Protoc.* 10 (2014) (2014) pdb prot080028.
- [25] B. Hollenbach, N.G. Morgenthaler, J. Struck, C. Alonso, A. Bergmann, J. Kohrle, L. Schomburg, New assay for the measurement of selenoprotein P as a sepsis biomarker from serum, *J. Trace Elem. Med. Biol.* 22 (1) (2008) 24–32.
- [26] P. Italiani, E.M. Mazza, D. Lucchesi, I. Cifola, C. Gemelli, A. Grande, C. Battaglia, S. Bicciato, D. Boraschi, Transcriptomic profiling of the development of the inflammatory response in human monocytes in vitro, *PLoS One* 9 (2) (2014), e87680.
- [27] M. Orecchioni, Y. Ghosheh, A.B. Pramod, K. Ley, Macrophage polarization: different gene signatures in M1(LPS+) vs. Classically and M2(LPS-) vs. Alternatively activated macrophages, *Front. Immunol.* 10 (2019) 1084.
- [28] S. Saha, I.N. Shalova, S.K. Biswas, Metabolic regulation of macrophage phenotype and function, *Immunol. Rev.* 280 (1) (2017) 102–111.
- [29] L.J. Huang, X.T. Mao, Y.Y. Li, D.D. Liu, K.Q. Fan, R.B. Liu, T.T. Wu, H.L. Wang, Y. Zhang, B. Yang, C.Q. Ye, J.Y. Zhong, R.J. Chai, Q. Cao, J. Jin, Multiomics analyses reveal a critical role of selenium in controlling T cell differentiation in Crohn's disease, *Immunity* 54 (8) (2021) 1728–1744, e7.
- [30] F.H. Hawker, P.M. Stewart, P.J. Snitch, Effects of acute illness on selenium homeostasis, *Crit. Care Med.* 18 (4) (1990) 442–446.
- [31] X. Forceville, D. Vitoux, R. Gauzit, A. Combes, P. Lahilaire, P. Chappuis, Selenium, systemic immune response syndrome, sepsis, and outcome in critically ill patients, *Crit. Care Med.* 26 (9) (1998) 1536–1544.
- [32] K. Renko, P.J. Hofmann, M. Stoedter, B. Hollenbach, T. Behrends, J. Kohrle, U. Schweizer, L. Schomburg, Down-regulation of the hepatic selenoprotein biosynthesis machinery impairs selenium metabolism during the acute phase response in mice, *Faseb. J.* 23 (6) (2009) 1758–1765.
- [33] T. Suzuki, V.P. Kelly, H. Motohashi, O. Nakajima, S. Takahashi, S. Nishimura, M. Yamamoto, Deletion of the selenocysteine tRNA gene in macrophages and liver results in compensatory gene induction of cytoprotective enzymes by Nrf2, *J. Biol. Chem.* 283 (4) (2008) 2021–2030.
- [34] N.J. Darling, R. Toth, J.S. Arthur, K. Clark, Inhibition of SIK2 and SIK3 during differentiation enhances the anti-inflammatory phenotype of macrophages, *Biochem. J.* 474 (4) (2017) 521–537.
- [35] A. Yurdagul, M. Subramanian, X. Wang, S.B. Crown, O.R. Ilkayeva, L. Darville, G. K. Kolluru, C.C. Rymond, B.D. Gerlach, Z. Zheng, G. Kuriakose, C.G. Kevil, J. M. Koomen, J.L. Cleveland, D.M. Muoio, I. Tabas, Macrophage metabolism of apoptotic cell-derived arginine promotes continual efferocytosis and resolution of injury, *Cell Metabol.* 31 (3) (2020) 518–533, e10.
- [36] A.M. Korwar, A.E. Shay, V. Basrur, K. Conlon, K.S. Prabhu, Selenoproteome identification in inflamed murine primary bone marrow-derived macrophages by nano-LC orbitrap fusion tribrid mass spectrometry, *J. Am. Soc. Mass Spectrom.* 30 (7) (2019) 1276–1283.
- [37] A.R. Watson, H. Dai, Y. Zheng, R. Nakano, A.D. Giannou, A.V. Menk, D.B. Stolz, G. M. Delgoffe, A.W. Thomson, mTORC2 deficiency alters the metabolic profile of conventional dendritic cells, *Front. Immunol.* 10 (2019) 1451.